Structural and Kinetic Evidence for Strain in Biological Catalysis[†,‡]

Floyd E. Romesberg,[§] Bernard D. Santarsiero,[||] Ben Spiller,[||] Jun Yin,[§] Dwight Barnes,[||] Peter G. Schultz,*[,§] and Raymond C. Stevens*[,||]

Howard Hughes Medical Institute and Department of Chemistry, University of California, Berkeley, Berkeley, California 94720

Received July 2, 1998; Revised Manuscript Received August 7, 1998

ABSTRACT: A classic hypothesis for enzyme catalysis is the induction of strain in the substrate. This notion was first expressed by Haldane with the lock and key analogy—"the key does not fit the lock perfectly but exercises a certain strain on it" (*1*). This mechanism has often been invoked to explain the catalytic efficiency of enzymes but has been difficult to establish conclusively (*2*−*7*). Here we describe X-ray crystallographic and mutational studies of an antibody metal chelatase which strongly support the notion that this antibody catalyzes metal ion insertion into the porphyrin ring by inducing strain. Analysis of the germline precursor suggests that this strain mechanism arose during the process of affinity maturation in response to a conformationally distorted *N*-alkylmesoporphyrin.

N-Alkylporphyrins are metalated at rates which are orders of magnitude faster than their nonalkylated analogues (*8*). This is thought to result from distortion of the planar porphyrin ring toward a transition state-like geometry by the *N*-alkyl substituent. *N*-Alkylporphyrins are also strong inhibitors of the enzyme ferrochelatase (*9*), which catalyzes the insertion of metal ions into porphyrin, a key step in heme biosynthesis. These observations have led to the proposal that ferrochelatase functions by straining the porphyrin ring toward a distorted conformation in which the two pyrrole N-σ electrons are more accessible to metal ions (*10*). Consistent with this notion, antibody 7G12, raised against a distorted *N*-alkylmesoporphyrin **1**, was found to catalyze Cu(II) insertion into mesoporphyrin substrate **2** with a catalytic efficiency approaching that of ferrochelatase (Figure 1) (*11*). To establish the structural basis for catalysis by antibody 7G12, X-ray crystallographic and mutagenesis studies were carried out along with characterization of mutations along the path of affinity maturation from the germline precursor antibody to 7G12.

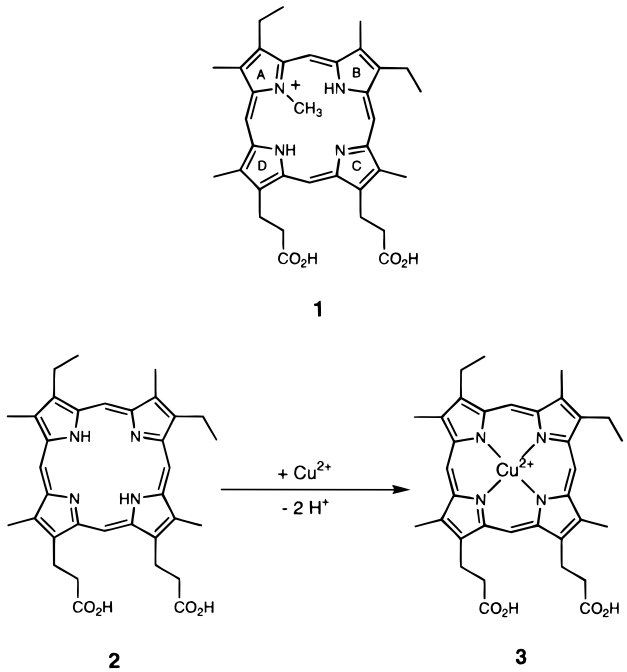

FIGURE 1: *N*-Methylmesoporphyrin (hapten **1**) and mesoporphyrin metalation reaction catalyzed by antibody 7G12.

EXPERIMENTAL PROCEDURES

Antibody Cloning and Mutagenesis. Total RNA was isolated from the hybridoma cell line by the method of Chomczynski and Sacchi (*12*). Total RNA was enriched for messenger RNA coding for 7G12 or 5A5 variable regions by affinity chromatography with oligo(dT) cellulose (Pharmacia). Constant region 3′ primers were used to reverse transcribe cDNA. PCR[1] amplification with the 3′ constant region primer and the 5′ primers described by Huse et al. (*13*) yielded sufficient DNA for cloning and sequencing. After determination of the J_κ and J_H regions used by 7G12 and 5A5, 3′ primers corresponding to the respective J regions and containing restriction sites were synthesized and used in conjunction with the 5′ primers to PCR amplify DNA

[†] This work was supported by National Institutes of Health Grants R01 AI24695 (P.G.S.) and R01 AI39089 (R.C.S.) and The Director, Office of Energy Research, Office of Biological and Environmental Research, General Life Sciences Division of the U.S. Department of Energy, under Contract DE-AC03-76SF00098. P.G.S. is a Howard Hughes Medical Institute Investigator and a W.M. Keck Foundation Investigator.

[‡] The coordinates have been deposited with the Brookhaven Protein Data Bank, accession number 3fct.

* To whom correspondence should be addressed.

[§] Howard Hughes Medical Institute.

[||] Department of Chemistry.

[1] Abbreviations: Tris, tris(hydroxymethyl)aminomethane; PCR, polymerase chain reaction; Fab, fragment, antigen binding; PEG, poly(ethylene glycol); DMSO, dimethyl sulfoxide; CDR, complementarity-determining region.

S0006-2960(98)01578-5 CCC: $15.00
Published on Web 09/22/1998

corresponding to the antibody variable regions. The V_H and V_L genes were cloned into plasmid p4X (*14*). To facilate cloning, the following mutations were introduced into the 5′ end of the V_L region: $Asp1^L$ to Glu, $Ile2^L$ to Leu, $Ser7^L$ to Thr, and $Gln8^L$ to Pro. This construct fuses the murine V_H and V_L genes to human C_H1 and $C_\kappa1$ constant regions, respectively, yielding a chimeric Fab. The Fab fragments were isolated from *E. coli* 25F2 cells transformed with the appropriate plasmids, according to the published protocol (*14*). Fab fragments were purified by protein G affinity chromatography (Sepharose CL-6B, Pierce). For crystallization, the protein was further purified by ion exchange chromatography (HS Poros), then incubated with 10-fold excess of *N*-methylmesoporphyrin, and further purified by gel filtration on a Superdex S-200 column (Pharmacia) equilibrated with 100 mM NaCl, 10 mM Tris (pH 7.5), 1 mM methionine. Purified Fab was concentrated in an Amicon cell to roughly 15 mg/mL. For kinetic experiments, protein G affinity purified Fab fragments were dialyzed against high salt buffer (0.5 M NaCl, 10 mM Na_2HPO_4, pH 7.5) and incubated at room temperature overnight with hemin−agarose resin (Sigma) as a 50% suspension in the same buffer. The suspension was then packed into a column and washed extensively with high salt buffer. Fab fragments were eluted (7 M guanidine hydrochloride, 50 mM Na_2HPO_4, pH 7.5) and dialyzed against binding buffer followed by protein G affinity chromatography. The antibodies were concentrated and stored in either kinetics buffer or phosphate buffered saline (Ca^{2+}, Mg^{2+} free, deionized water).

Cloning of the Germline Precursor Antibody. Coding region sequence homology was used to identify candidate germline genes from the Kabat database (*15*). Based on published sequences [V_{TNP} (*16*) and B4 (*17*)], 5′-PCR primers were designed to anneal to upstream untranslated DNA. These primers, in conjunction with J region specific 3′ primers, were used for PCR amplification with DNA isolated from either a Swiss-Webster spleen or 7G12 hybridoma cells. PCR products were then cloned and sequenced. Sequence was determined 311 and 400 nt upstream for the light and heavy chains, respectively, to uniquely identify the germline gene.

Crystallization and Structure Determination. Crystals of recombinant Fab with diastereomeric *N*-methylmesoporphyrin were obtained by the hanging drop method at 20 °C using 27% PEG-2K-mme, 200 mM ammonium sulfate, 100 mM Tris (pH 7.0), and 10 mM cadmium sulfate. Crystals were frozen from mother liquor, and X-ray diffraction data were collected at Brookhaven National Laboratory NSLS at −170 °C on beamline X-12C to a resolution of 2.4 Å. The space group was found to be $P2_12_12$ with unit cell parameters a = 134.70 Å, b = 100.83 Å, c = 73.56 Å, and two Fab molecules per asymmetric unit. The average mosaic spread was found to be relatively large, and set at 0.80°. DENZO (*18*) was used to index and integrate the 134 467 intensities to 2.40 Å. Scaling with SCALEPACK (*18*) led to 33 863 unique intensities, 98.4% complete to 2.8, 85.9% complete overall to 2.4 Å, with an overall *R*(merge) of 0.081. The structure was determined by molecular replacement using antibody 48G7 (*19*). AMoRe (*20*) was used to determine the relative orientation and position of the search model (either a single variable or a constant domain) for each Fab in the asymmetric unit. The coordinates from a previously reported Fab structure were used to generate the search model of the Fab by variation of the elbow angle (*19*). The best solution was found using the 10−4 Å intensities, with a Patterson radius of 25−30 Å. The structure was refined using X-PLOR 3.851 and CNS (*21*, *22*), first with rigid-body domains, and then positional and individual isotropic *B* shifts. Electron density maps were generated with use of the CCP4 package (*23*), and manual rebuilding through the use of O (*24*). *R*(cryst) is 20.6% and *R*(free) is 29.3% with the 20.0−2.4 Å data. Each Fab molecule is composed of a light chain with 213 residues, and a heavy chain with 216 residues. The hapten was generated by idealization of two reported *N*-methylmesoporphyrin structures (*25*, *26*). The porphyrin ring is bound in a nonplanar geometry with a clear distortion of one pyrrole ring out of the plane of the rest of the porphyrin molecule (Figures 2 and 3). To confirm this geometry, a simulated annealing electron density omit map was generated without hapten in the model; the resulting electron density for the porphyrin was once again observed to be nonplanar (Figure 3). A total of 546 water molecules were added to the model to improve the fit to the electron density. Molecular surfaces and surface areas were calculated by using the program MS (*27*) with a 1.6 Å probe radius and extended atom van der Waals radii (*28*). The pairwise contacts between antibody and hapten were determined by the method of Sheriff and extended atom van der Waals radii (*29*).

Kinetics Analysis. Kinetics of the copper insertion reaction were monitored at 497 nm (disappearance of starting porphyrin) and at 559 nm (appearance of metalated porphyrin) on a Uvikon 933 double beam UV/Vis spectrophotometer. Kinetics were measured in 100 mM Tris acetate (pH 8.0), 5% DMSO, 0.5% Triton X-100. The Fab concentration was 0.5 or 1 μM, copper acetate was 1 mM, and the mesoporphyrin concentration was varied. After correction for background, initial catalyzed velocities were determined and fit to the Michaelis−Menten equation.

RESULTS AND DISCUSSION

Antibody 7G12 was cloned from hybridoma cells and expressed in active form [k_{cat} = 24.8 h^{-1}, K_M = 150 μM for Cu(II) insertion] as a chimeric Fab by fusion of the V_H and V_L genes to human C_H1 and Cκ1 constant regions, respectively (*14*). The three-dimensional crystal structure of the complex of the Fab fragment of 7G12 and *N*-methylmesoporphyrin **1** was determined to 2.4 Å. Well-defined electron density is observed for hapten **1** at 2.5σ. The structure shows that the *N*-methylmesoporphyrin is bound in an unsymmetrical, shallow cleft between the antibody V_H and V_L domains (Figures 2 and 3). Approximately 390 Å^2 of the hapten is buried in the combining site: there are 114 pairwise contacts between hapten **1** and 7G12. The propionate groups of **1** are directed into solvent and appear to form no specific contacts with the Fab. Heavy chain hypervariable loops H1 and H3 combine to form a large surface that contacts an entire face of the porphyrin ring, while light chain hypervariable loop L3 forms an opposing smaller surface that contacts only pyrrole rings A and B. The porphyrin is bound predominantly by hydrophobic contacts with the active site residues $Tyr36^L$, $Leu46^L$, $Tyr49^L$, $Tyr55^L$, $Gln89^L$, $Tyr91^L$, $Tyr94^L$, $Leu96^L$, $Trp33^H$, $Met50^H$, and $Met97^H$.

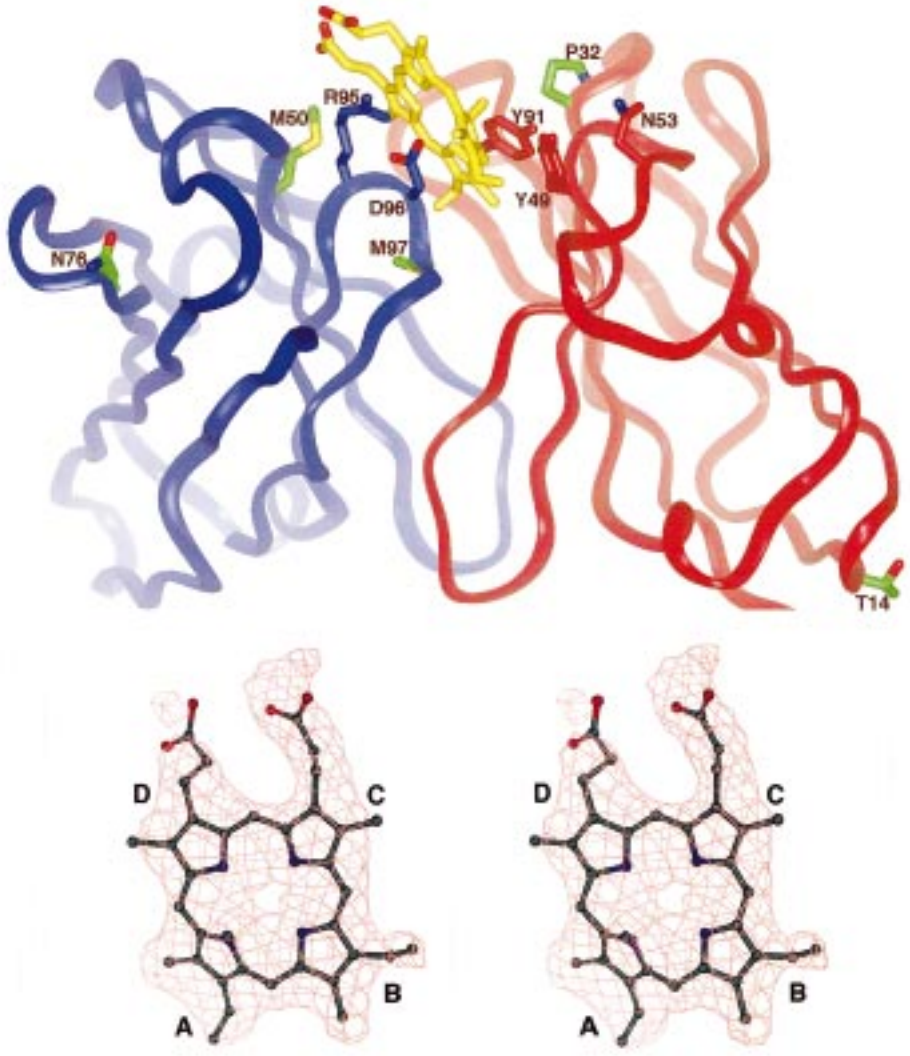

FIGURE 2: (Top) Three-dimensional structure of the variable region domain of the complex of the 7G12 Fab fragment with hapten **1**. Critical side chains are colored as follows: somatic mutations Thr14^{L}, Pro32^{L}, Met50^{H}, Asn76^{H}, and Met97^{H}, green; Arg95^{H} and Asp96^{H}, blue; and Tyr49^{L}, Asn53^{L}, and Tyr91^{L}, red. Hapten is colored yellow. (Bottom) Stereodiagram of $F_o - F_c$ electron density map, illustrating the electron density in the antibody combining site. The electron density map was contoured at 2.5σ.

The $F_o - F_c$ electron density map shows principally electron density for the hapten isomer with pyrrole ring A *N*-methylated and does not show significant density for any of the other *N*-methylated isomers (an isomeric mixture was used for crystallization). Packing interactions between the hapten and the V_L domain residues Tyr49^{L} and Tyr91^{L} appear to play an important role in binding the distorted conformation of *N*-methylmesoporphyrin. Tyr91^{L} π-stacks on pyrrole ring B, which is coplanar with the solvent-exposed pyrrole rings C and D. Tyr49^{L} π-stacks on pyrrole ring A, which is distorted out of the plane of the other pyrrole rings by approximately 42°. Packing interactions between both tyrosine side chains and the porphyrin ring are reinforced by interactions with other antibody side chains. Tyr91^{L} and Tyr49^{L} are packed tightly with the side chains of Pro32^{L} and Asn53^{L}, respectively (Figure 3), and the aryl oxygen of Tyr49^{L} is also hydrogen bonded to the carboxamide side chain of Asn53^{L}. From the V_H side of the binding pocket, pyrrole rings B, C, and D are packed tightly against Arg95^{H}, Asp96^{H}, and Met97^{H}; however, there is a noticeable absence of packing interactions between pyrrole ring A and the V_H domain. Thus, residues Tyr49^{L} and Tyr91^{L} are preorganized to pack against one face of pyrrole rings A and B, respectively, and are opposed from the V_H face by Met97^{H} at pyrrole ring B. The opposing nature of the packing interactions of Tyr91^{L} and Met97^{H} on opposite sides of pyrrole ring B may act as a clamp to fix its position. Because there is no residue on the opposite face of pyrrole ring A to oppose a distorting force by Tyr49^{L}, ring A is activated for distortion. This conclusion is consistent with recent resonance Raman experiments which showed that antibody 7G12 induces distortion in the bound mesoporphyrin substrate corresponding to an alternating up-and-down tilting of two opposite pyrrole rings (*30*). Moreover, the distortions of the porphyrin induced by the antibody combining site are identical to distortions induced by *N*-methylation of the free mesoporphyrin. The precise degree to which the strain induced by unfavorable packing interactions with active site residues is manifested in the conformation of the bound substrate requires determination of the three-dimensional structure of the Michaelis complex.

The crystal structure also shows that the carboxylate OD1 of Asp96^{H} is roughly equidistant from the four pyrrole nitrogen atoms of **1** (2.7−3.1 Å), and approximately 1.9 Å

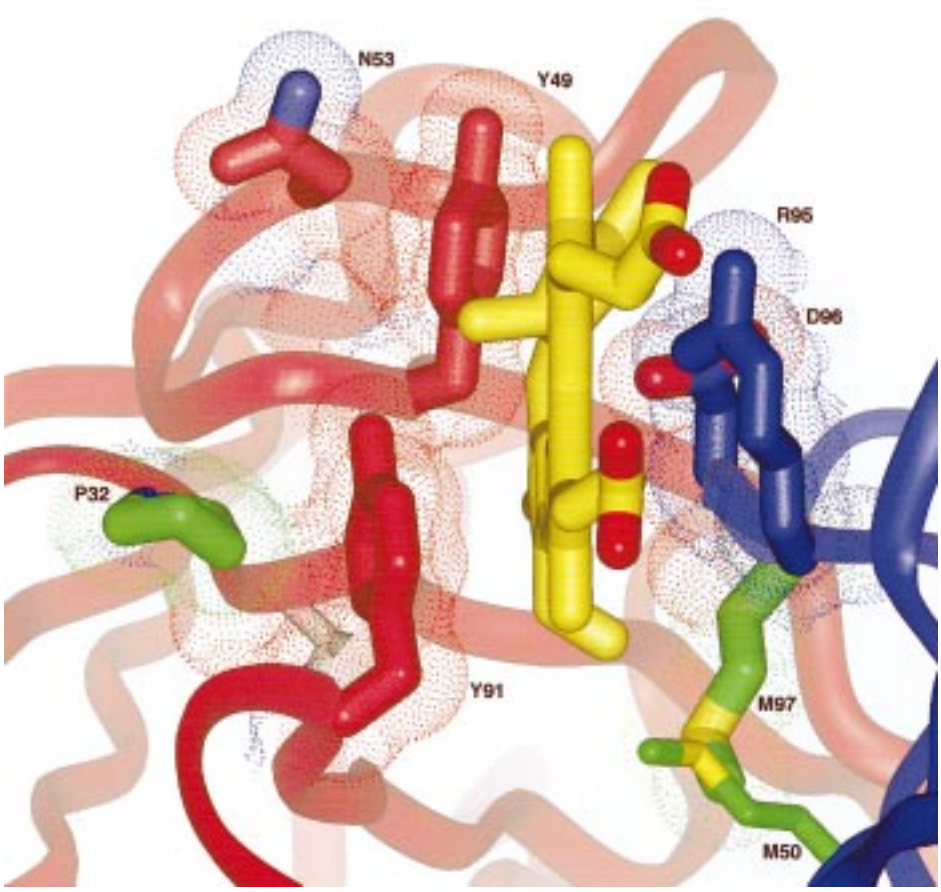

FIGURE 3: Illustration of antibody 7G12 and packing interactions with hapten **1**; hapten is colored yellow. Antibody side chains Tyr49^{L}, Asn53^{L}, and Tyr91^{L} are colored red; Arg95^{H} and Asp96^{H} are colored blue; Pro32^{L}, Met50^{H}, and Met97^{H} are colored green.

from the center of the porphyrin ring. The Asp96^{H} carboxylate side chain is positioned by a hydrogen bond from Arg95^{H} to OD2 (Figure 2). Mutants were generated with Ala, His, or Asn at heavy chain position 96 in order to examine the potential role of Asp96^{H} in catalysis. None of the mutants catalyzed Cu(II) ion insertion to any measurable extent, demonstrating the absolute requirement of Asp96^{H} for catalytic activity. However, it is unclear whether Asp96^{H} is acting as a general base to shuttle protons from the porphyrin during metal ion exchange, or if it is directly participating in Cu(II) insertion by formation of a metal−oxo bond. In the latter case, the hydrogen bond between Asp96^{H} and Arg95^{H} may act to reduce the entropic cost of losing rotational degrees of freedom upon metal ion complexation. Mutagenesis of Asp96^{H} to other metal chelating residues may help to further define its role, as well as to possibly introduce oxygen binding and activation activities into the antibody.

Somatic mutations are introduced in the variable region during affinity maturation in order to increase the binding affinity of antibody for antigen. To evaluate the contributions of these natural "affinity" selected mutations to catalysis, the germline precursor antibody (no somatic mutations) to 7G12 was cloned. The sequences of the light and heavy chain germline genes, isolated from Swiss-Webster mouse spleen cells, and the corresponding affinity matured 7G12 genes, isolated from hybridoma DNA, are shown in Figure 4. Also shown in Figure 4 is the sequence of antibody 5A5, which was also isolated in response to hapten **1** and shown to catalyze Cu(II) insertion (*11*). It is evident that 7G12 and 5A5 resulted from the same clonal expansion and are thus related by somatic mutations, with 5A5 having fewer mutations. We were unable to differentiate between two V_H germline genes which differed at a single amino acid in the coding region (Asn or Arg at residue 50) which was somatically mutated to Met50^{H} in 7G12. There are two additional mutations in the 7G12 V_H chain, Ser to Asn at position 76 and Ser to Met at position 97. Antibody 7G12 has two somatic mutations in V_L, Ser to Thr at position 14 and Ala to Pro at position 32. The V_H residues Met97^{H} and Asn76^{H} are 3.4 and 21 Å from the hapten, respectively, while the V_κ residues Thr14^{L} and Pro32^{L} are 29 and 7.6 Å from the hapten, respectively. The mechanistically important residues Tyr49^{L}, Tyr91^{L}, Asn53^{L}, and Arg95^{H} are encoded in the germline DNA. Asp96^{H} in CDRH3 is coded for by DNA randomly inserted during recombination (P/N sequence), and we are therefore not able to determine whether the origin of this residue is the germline DNA or a somatic mutation.

Analysis of the structure of the 7G12 Fab·*N*-methylmesoporphyrin complex suggests that residues Pro32^{L} and Met97^{H}, which were introduced during affinity maturation in response to hapten **1**, may play a central role in distorting the porphyrin substrate toward the reactive, bent conformation. Consequently, the contributions of these mutations to catalysis were examined by generating the individual Pro32^{L}-

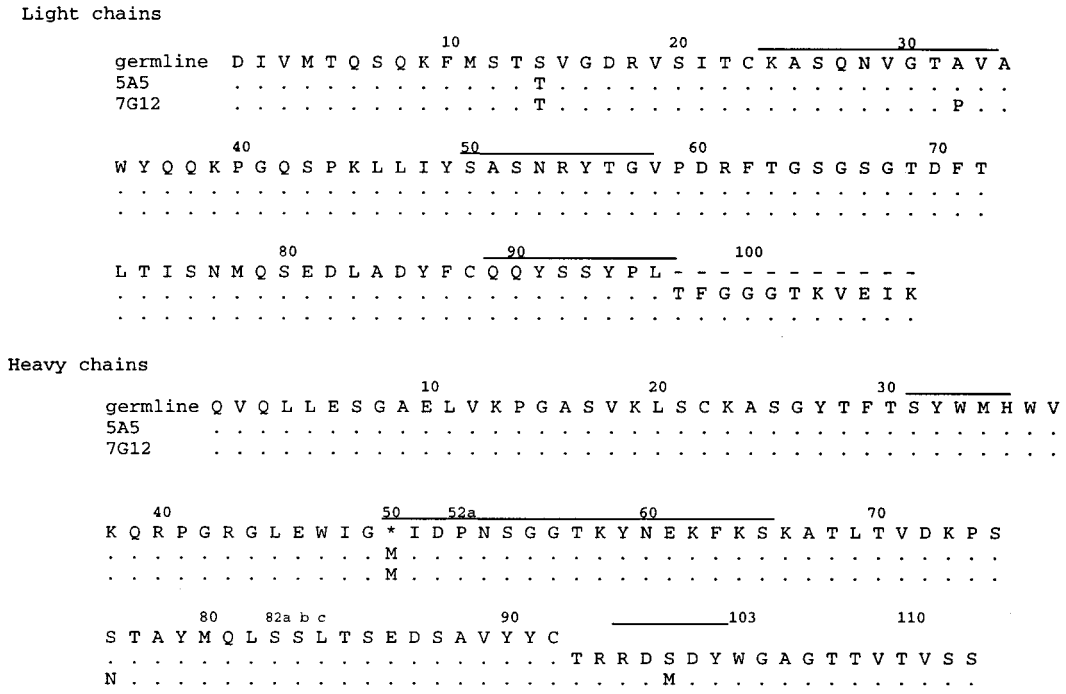

FIGURE 4: Light and heavy chain variable region sequences of 7G12, 5A5, and their germline precursors.

Ala and Met97^{H}Ser mutants by site-directed mutagenesis. The Pro32^{L}Ala mutant possessed a virtually unchanged k_{cat} of 37 h^{-1} but a significantly increased K_M of 400 μM. Apparently, the contribution of Pro32^{L} to substrate binding is not differentially manifested in the ground and transition states. The Met97^{H}Ser "germline" mutant was also able to catalyze the insertion of Cu(II) into mesoporphyrin, but with a reduced k_{cat} of 2.2 h^{-1} and a K_M of 191 μM. This single somatic mutation, generated in response to *N*-methylmesoporphyrin **1**, increases k_{cat} by more than an order of magnitude while leaving K_M virtually unchanged. The fact that the Ser97^{H} and Met97^{H} antibodies have similar binding affinities for the planar substrate, but differ in affinity for the distorted transition state by approximately 1.4 kcal/mol, indicates that the strain induced at the A and B pyrrole rings is manifested largely in the transition state. Specifically, mutation of Met97^{H} to Ser might release strain induced across the pyrrole rings A and B by the tyrosine residue on the opposing face of the porphyrin ring. Enzymes under selective pressure to achieve a maximal rate of catalysis will evolve by increasing k_{cat}/K_M while maintaining the largest possible K_M (*31*). This prevents the enzyme−substrate complex from becoming a "thermodynamic trap" and maximizes the rate of product formation. In this sense, the somatic mutation from Ser97^{H} to Met97^{H} represents an optimal mutation to enhance catalytic efficiency, showing that somatic mutation and clonal selection, like natural evolution, can evolve increasingly efficient catalysts when programmed with appropriate mechanistic information.

In an attempt to further investigate this strain mechanism, we generated the Tyr49^{L}Ala and Tyr91^{L}Ala mutants. However, an increased K_M and limited substrate solubility precluded the saturation of the antibody with porphyrin; therefore, only k_{cat}/K_M values were determined. The specificity constants of the Tyr49^{L}Ala and Tyr91^{L}Ala mutants were 1.90×10^{-2} h^{-1} μM^{-1} and 4.76×10^{-3} h^{-1} μM^{-1}. While not providing kinetic evidence directly favoring their preferential binding to a distorted substrate, the 10- and 40-fold decreased second-order rate constants of these mutants are consistent with the role of these tyrosine residues suggested by the structural data.

The crystal structure of the *B. subtilis* ferrochelatase without ligand has recently been reported and provides the opportunity to compare two biological catalysts with very different structures but similar functions (*32*). The 310 amino acid ferrochelatase folds into 2 Rossman-like domains. The high sequence homology of the domains has led to the suggestion that they evolved from a common ancestral gene that underwent a tandem gene duplication (*32*). However, each domain contains three regions which have diverged considerably, both in sequence and in length. Two of these regions, $\alpha 1_I$-loop-$\alpha 2_I$ and loop $\beta 2_{II}/\alpha 3_{II}$, protrude from the core of the molecule opposite one another, and form a major component of a hydrophobic cleft between the two domains where porphyrin presumably binds. Amino acid residues contained within these loops, as well as several additional residues from each domain, are predicted to contact the porphyrin and have been shown by mutagenesis to be important for catalytic function. Gold and cadmium ions were bound by a single Nϵ2 of a histidine residue, whose catalytic role has also been implicated in mutagenesis studies.

Antibody 7G12 shows no sequence homology to *B. subtilis* ferrochelatase, but it does have a combining site with several important similarities to the enzyme (*33*). Both proteins present a hydrophobic binding cleft formed by hypervariable loops between two similar domains. Both structures show critical hydrophobic residues that pack against the loops involved in binding porphyrin, Trp230 in ferrochelatase and Pro32^{L} and Asn53^{L} in 7G12. Porphyrin binds (or is predicted to bind, in the case of ferrochelatase) edge-on in the cleft with propionic groups oriented into solvent, burying pyrrole rings A and B in the binding pocket. Resonance Raman experiments suggest that the enzyme, like the antibody, distorts the porphyrin ring, but in a doming

motion rather than the up and down distortion induced by 7G12 (*30*). Both ferrochelatase and 7G12 bind metal ions with an active site residue: Nϵ2 of His and OD1 of Asp, respectively. A difference between the two catalysts is the presence of a basic residue in ferrochelatase which is postulated to deprotonate the substrate prior to metal insertion. No such base is obvious in the 7G12 structure, although the carboxylate side chain of $Asp96^{H}$ may act both to deprotonate substrate and to chelate metal.

The structural and functional homologies of ferrochelatase and 7G12 are remarkable when considered in the context of the immune system's ability to generate catalysts. Starting from the combinatorial diversity of the antibody germline gene repertoire and using affinity maturation, the immune system is able to produce a catalyst within weeks that is remarkably similar to a biosynthetic enzyme.

REFERENCES

1. Haldane, J. B. S. (1930) *Enzymes*, Longmans, Green and Co., London.
2. Blake, C. C. F., et al. (1967) *Proc. R. Soc. London* B167, 378.
3. Belasco, J. G., and Knowles, J. R. (1980) *Biochemistry 19*, 472.
4. Robillard, G., Shaw, E., and Shulman, R. G. (1974) *Proc. Natl. Acad. Sci. U.S.A. 71*, 2623.
5. Fersht, A. R., Blow, D. M., and Fastrez, J. (1973) *Biochemistry 12*, 2035.
6. Dunitz, J. D., and Winkler, F. K. (1975) *Acta Crystallogr. B 31*, 251.
7. Phillips, D. C. (1967) *Proc. Natl. Acad. Sci. U.S.A. 57*, 484.
8. Bain-Ackerman, M. J., and Lavallee, D. K. (1979) *Inorg. Chem. 18*, 3358.
9. Dailey, H. A., and Fleming, J. E. (1983) *J. Biol. Chem. 258*, 11453.
10. McLaughlin, G. M. (1974) *J. Chem. Soc., Perkin Trans. 2* 136.
11. Cochran, A. G., and Schultz, P. G. (1990) *Science 249*, 781.
12. Chomczynski, P., and Sacchi, N. (1987) *Anal. Biochem. 162*, 156.
13. Huse, W. D., et al. (1989) *Science 246*, 1275.
14. Ulrich, H. D., et al. (1995) *Proc. Natl. Acad. Sci. U.S.A. 92*, 11907.
15. Kabat, E. A., Wu, T. T., Perry, H. M., Gottersman, K. S., and Fowler, C. (1991) *Sequences of Proteins of Immunological Interest* (U.S. Department of Health and Human Services, National Institutions of Health, Bethesda, MD.
16. Hawley, R. G., et al. (1982) *Proc. Natl. Acad. Sci. U.S.A. 79*, 7425.
17. Yankopoulos, G. D., and Alt, F. W. (1985) *Cell 40*, 271.
18. Otwinowski, Z., and Minor, W. (1996) *Methods Enzymol. 276*, 307.
19. Wedemayer, G. J., et al. (1997) *J. Mol. Biol. 268*, 390.
20. Navaza, J. (1994) *Acta Crystallogr. A 50*, 157.
21. Brunger, A. T. (1996) X-PLOR, *Version 3.851. A System for X-ray Crystallography and NMR*, Yale University Press, New Haven, CT.
22. Brunger, A. T. et al. (1998) *CNS version 0.3*.
23. Collaborative Computational Project Number 4 (1994) *Acta Crystallogr. D 50*, 760.
24. Jones, T. A., Zou, J.-Y., Cowan, S. W., and Kjeldgaard, M. (1991) *Acta Crystallogr. A 47*, 110.
25. Lavallee, D. K., and Anderson, O. P. (1982) *J. Am. Chem. Soc. 104*, 4707.
26. Aizawa, S., Tsuda, Y., Ito, Y., Hatano, K., and Funahashi, S. (1993) *Inorg. Chem. 32*, 1119.
27. Connolly, M. L. (1983) *J. Appl. Crystallogr. 20*, 517.
28. Gelin, B. R., and Karplus, M. (1979) *Biochemistry 18*, 1256.
29. Sheriff, S., Hendrickson, W. A., and Smith, J. L. (1987) *J. Mol. Biol. 197*, 273.
30. Blackwood, M. E., Jr., Rush, T. S., Romesberg, F., Schultz, P. G., and Spiro, T. G. (1998) *Biochemistry 37*, 779.
31. Fersht, A. (1985) *Enzyme Structure and Mechanism*, Chapter 12, W. H. Freeman and Co., New York.
32. Al-Karadaghi, S., Hansson, M., Stanislav, N., Johnson, B., and Hederstedt, L. (1997) *Structure 5*, 1501.
33. Raux, E., Thermes, C., Heathcote, P., Rambach, A., and Warren, M. J. (1997) *J. Bacteriol. 179*, 3202.

BI981578C